ELSEVIER

Materials Science and Engineering A 426 (2006) 274–277

MATERIALS SCIENCE & ENGINEERING A

www.elsevier.com/locate/msea

Characteristics of nano Ti-doped SnO_2 powders prepared by sol–gel method

X.M. Liu [a,b], S.L. Wu [a,b], Paul K. Chu [a,*], J. Zheng [b], S.L. Li [b]

[a] *Department of Physics & Materials Science, City University of Hong Kong, Kowloon, Hong Kong*
[b] *School of Materials Science and Engineering, Tianjin University, Tianjin 300072, China*

Received 20 June 2005; received in revised form 29 March 2006; accepted 12 April 2006

Abstract

Ti^{4+}-doped SnO_2 nano-powders were prepared by the sol–gel process using tin tetrachloride and titanium tetrachloride as the starting materials. The crystallinity and purity of the powders were analyzed by X-ray diffraction (XRD) and the size and distribution of Ti^{4+}-doped SnO_2 grains were studied using transmission electron microscopy (TEM) and scanning electron microscopy (SEM). The results show that Ti^{4+} has been successfully incorporated into the SnO_2 crystal lattice and the electrical conductivity of the doped materials improves significantly.

PACS: 81.07.Wx

Keywords: Sol–gel; SnO_2; Titanium doping; Electrical conductivity

1. Introduction

$AgSnO_2$ contact materials are gradually replacing toxic AgCdO materials in switching devices such as contactors and circuit breakers [1,2] partly due to the more favorable properties of $AgSnO_2$ such as long lifetime, better welding resistance and less arc erosion [3]. Furthermore, growing environmental concerns have spurred the replacement of AgCdO by non-toxic $AgSnO_2$ [4]. However, $AgSnO_2$ suffers from inadequate welding behavior compared to AgCdO [5]. Generally, $AgSnO_2$ made by traditional metallurgical processes at high temperature exhibits high contact resistance caused by surface layers of accumulated SnO_2. This also leads to poor wettability of SnO_2 grains in the silver melt [6–9]. The large size and high hardness of SnO_2 particles prepared by traditional processes degrade the properties of $AgSnO_2$ contact materials [10].

The welding and thermal behavior of $AgSnO_2$ can be improved by incorporating oxides such as TeO_2, Cu_2O, Bi_2O_3 and W_2O_3 [5,11,12]. However, few studies have reported on the preparation and performance of tin oxide doped with ions such as Ti^{4+}. In this work, we prepared Ti^{4+}-doped SnO_2 using the sol–gel technique and investigated the microstructure, size, distribution and crystallization of Ti^{4+}-doped tin oxide grains as well as the effects of doped Ti^{4+} on the electrical conductivity of $AgSnO_2$.

2. Experimental details

The SnO_2 gel was prepared by the sol–gel technique [13,14]. Tin tetrachloride ($SnCl_4{\cdot}5H_2O$) was first dissolved in a solution composed of ethanol and de-ionized water (volume ratio is 1:1) to a concentration of 2 mol/l with vigorous stirring for 20 min. Titanium tetrachloride ($TiCl_4$) was then added to the solution with the dispersant of polyethylene glycol (PEG 400) and stirred for 30 min at 80 °C. The atomic ratio of Ti to Sn was 5:95. Ammonia was then added to the metal chloride solution until the pH of the mixture reached 7. After 48 h of aging in the air, the SnO_2 gel was centrifuged (Centrifugal machine, LD4-2, Beijing, China) at 3000 rpm for 5 min and only the solid gel was collected. In order to remove both the ammonia and chloride components, centrifugation in de-ionized water and ethanol was repeated until all chloride ions had been removed (by examining the centrifuged solution using 3 mol $AgNO_3$). The microstructure of the SnO_2 gels with and without the dispersant were evaluated using transmission electron microscopy (TEM, JEOL 100CXII).

The gel was then dried in an oven at 60 °C for 4 h to remove moisture. In order to investigate the effect of the treatment tem-

* Corresponding author. Tel.: +852 27887724; fax: +852 27889549.
E-mail address: paul.chu@cityu.edu.hk (P.K. Chu).

0921-5093/$ – see front matter © 2006 Elsevier B.V. All rights reserved.
doi:10.1016/j.msea.2006.04.032

perature on the particle size of Ti^{4+}-doped SnO_2 powders, the dried gel was sintered for 2 h at 350, 500 and 700 °C in a furnace. To find the suitable particle size and crystallization, the morphologies of the Ti^{4+}-doped SnO_2 powders were studied by scanning electron microscopy (SEM; PHILIPS XL-30 TMP ESEM) and X-ray diffraction (XRD) patterns were obtained using a Rigaku X-ray diffractometer with a Cu Kα X-ray source operated at 40 kV and 100 mA.

Afterwards, the selected powders were passed through an 800 mesh sieve. In order to measure the electrical conductivity and density, 2.5 g of the Ti^{4+}-doped SnO_2 powders were compacted by hydraulic pressing at 100 MPa to make plates with a diameter of 9.3 mm. Because the solution temperature of SnO_2 was about 800 °C [15] the plates were calcined at 600, 800, 1000 and 1200 °C, respectively, about 2 h [16] to measure the change of electrical conductivity and density. The resistance of the plates was determined employing a bridge resistance instrument (LCR Databridge, KTJ-401D). The instrument was set in the resistance mode (*R*) and both probes were put on the two sides of the plate coated with some silver conductive paint. The resistance value of the plates was displayed on the screen and then the electrical conductivity of the plates was obtained by calculation. The density of these sintered plates was measured by Archimedes method in de-ionized water. The weight of the plates in air and water was determined respectively using an FR-300 MKI electronic balance with a precision of 0.1 mg. The density of the plates was then obtained according to ASTM B 328 [17] and ISO 2738 [18].

3. Results and discussion

The microstructure and distribution of the Ti^{4+}-doped SnO_2 gel grains are shown in Fig. 1. For the gel with polyethylene glycol (PEG) as the dispersant (Fig. 1a), it can be observed that the size of the grains varies from 10 to 100 nm and the grains are quite evenly distributed during gel formation. This indicates that PEG can effectively prevent the SnO_2 gel grains from agglomeration. Yang et al. [19] ascribed this phenomenon to the steric hindrance mechanism. With PEG as the dispersant, the gel particles can absorb long chain molecules of PEG on the surface, and it can inhibit the aggregation of the gel particles. Besides, the surface tension can be reduced due to the gel particles being surrounded by the PEG [20]. With regard to the gel formation without PEG, the gel particles in the solution are unstable because of their high surface tension. Moreover, the gel particles tend to agglomerate together without the interaction of steric hindrance. As shown in Fig. 1b, the Ti^{4+}-doped SnO_2 gel is poorly dispersed.

Fig. 2 displays the XRD spectra of the Ti^{4+}-doped SnO_2 powders sintered for 2 h at 350, 500 and 700 °C, respectively. The spectra indicate the presence of SnO_2 only and the peaks associated with Ti^{4+} cannot be observed. It reveals that Ti^{4+} has been successfully incorporated into the crystal lattice of SnO_2 by the sol–gel technique. As shown in Fig. 2, the intensity of the SnO_2 peaks increases with increasing treating temperature and the full-width half-maximum (FWHM) widths of the peaks decrease with increasing temperature as well. It indicates that crystallization of the SnO_2 powders progresses gradually as the

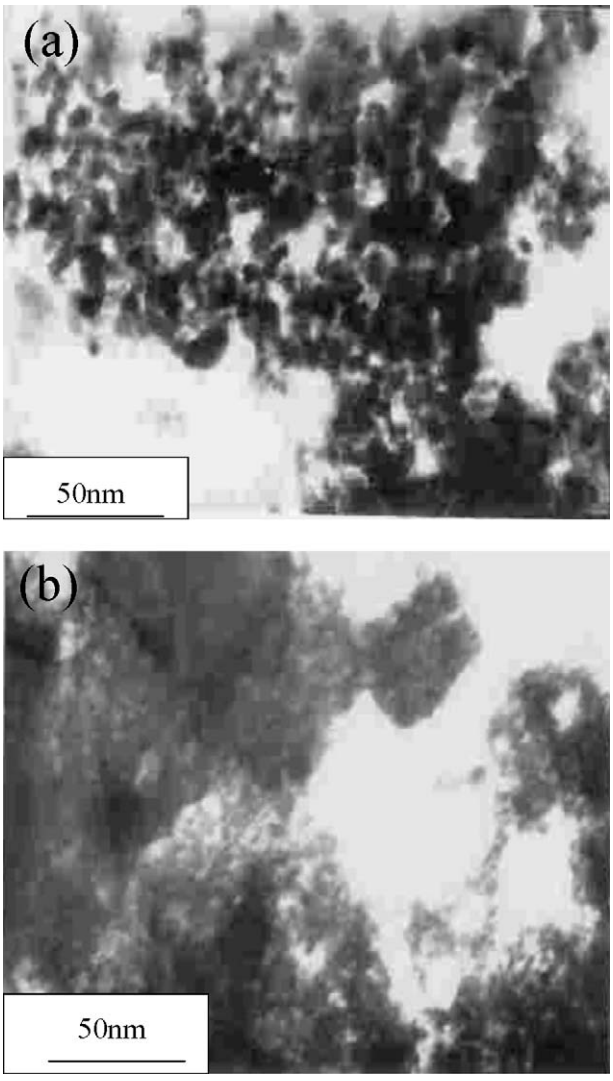

Fig. 1. TEM image of Ti^{4+}-doped tin oxide gel grains: (a) with PEG dispersant; (b) without PEG dispersant.

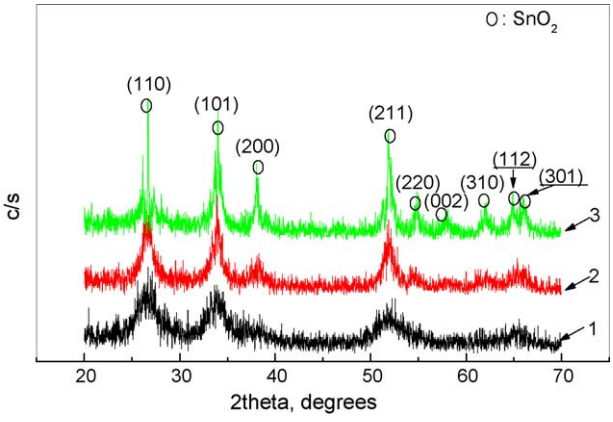

Fig. 2. XRD spectra of the Ti^{4+}-doped SnO_2 powders sintered for 2 h at different temperatures: 1, 350 °C; 2, 500 °C; 3, 700 °C.

Table 1
Grain size of Ti^{4+}-doped SnO_2 powders sintered at different temperatures

Temperature (°C)	Grain size (nm)
350	10–20
500	30–50
700	70–90

treating temperature increases. Our experimental data show that crystallization of the SnO_2 gel is not complete at a temperature of 350 °C, but perfect crystals can be obtained at higher treating temperatures at 500 and 700 °C. The grain size of the Ti^{4+}-doped SnO_2 powders treated at different temperatures can be obtained from the FWHM of the diffraction peaks. The FWHM's can be expressed as a linear combination of the contributions from the strain and particle size by the following equation [21]:

$$\frac{\beta \cos\theta}{\lambda} = \frac{1}{D} + \frac{\varepsilon \sin\theta}{\lambda}, \quad (1)$$

where β is the measured FWHM in radians, θ the Bragg angle of the diffraction peak, λ the X-ray wavelength, D the effective particle size and ε is the effective strain. The results are shown in Table 1. It can be concluded that the Ti^{4+}-doped SnO_2 powders sintered at 500 °C are more suitable because the grains aggregate easily at 700 °C, and it is supported by the SEM images shown in Fig. 3, which depicts the microstructure of the Ti^{4+}-doped SnO_2 powders sintered for 2 h at 500 and 700 °C. The grain size of the SnO_2 powders sintered at 700 °C is much larger than that of the powders sintered at a lower temperature. Furthermore, the grains

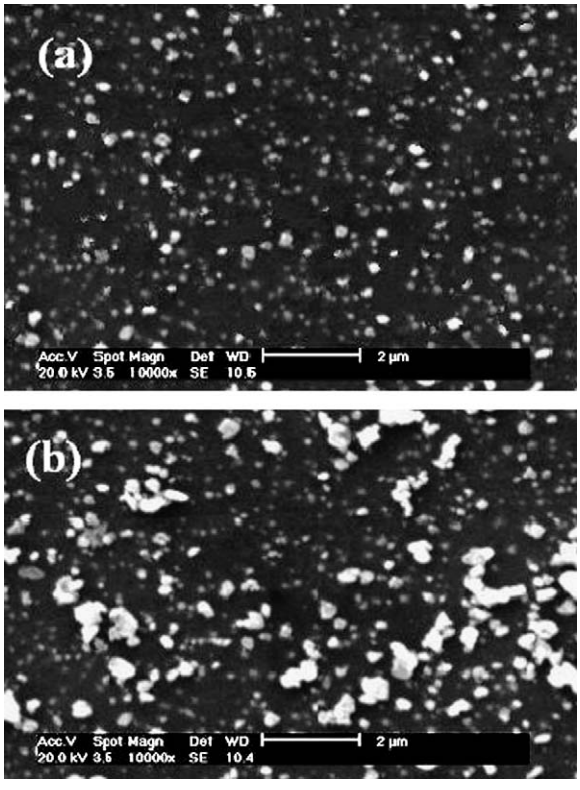

Fig. 3. SEM micrographs of Ti^{4+}-doped SnO_2 powders sintered at different temperatures for 2 h: (a) 500 °C and (b) 700 °C.

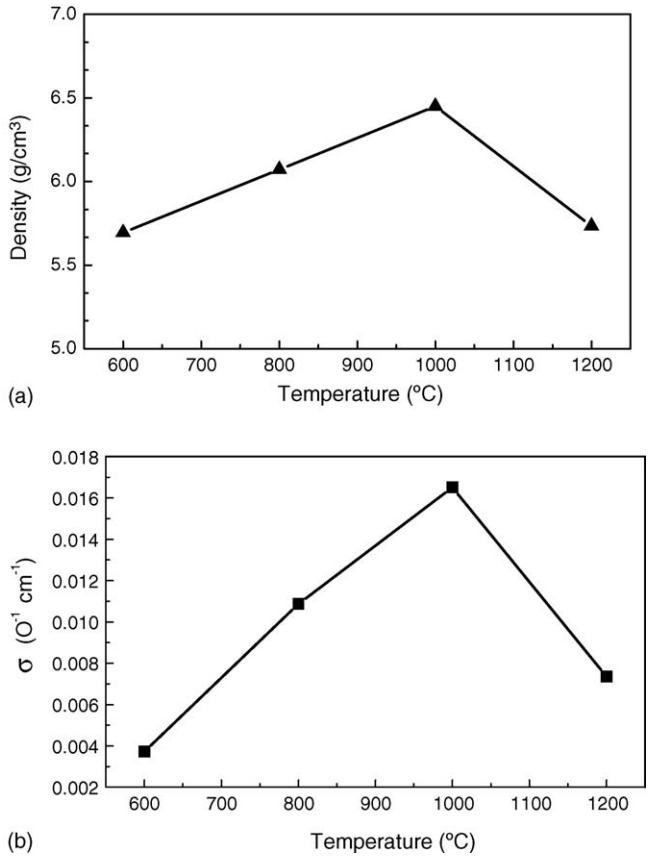

Fig. 4. Temperature dependence on density and electrical conductivity of Ti^{4+}-doped SnO_2: (a) density; (b) electrical conductivity.

in the sample sintered 500 °C are distributed evenly whereas those in the sample sintered at 700 °C exhibit agglomeration, which is very similar to ripening process [22,23]. At the expense of the small grains, some larger grains emerge. Hence, based on the above result, we chose the powders treated at 500 °C to conduct secondary calcination.

Fig. 4(a) and (b) show the graphs of the density and electrical conductivity of the Ti^{4+}-doped SnO_2 plates that have undergone secondary sintering at 600, 800, 1000 and 1200 °C. After calcination, the samples exhibit the highest density at 1000 °C. In the temperature range of 600–1000 °C, the density increases with higher temperature. This expansion is possibly caused by the growth of the grain and the reduction in the void content of the grain boundary. The samples sintered at a low temperature such as 600 °C, 800 °C show many voids in the grain boundary which can induce low electrical conductivity and density. Moreover the temperature is too low to make the solid solution of SnO_2 [15]. The higher temperature of about 1000 °C favors the solid solution of SnO_2 and eliminates the voids in the grain boundary. However, the density diminishes again when the temperature is up to 1200 °C because the higher temperature induces the rapid growth of the grains and increased voids along the grain boundary. As shown in Fig. 4(b), the electrical conductivity displays the similar trend with the density. The samples sintered at 1000 °C can achieve the highest electrical conductivity because the high density and successful solid solution can make the transfer of electron and vacancies easier.

Prepared by the same method, the density and electrical conductivity of the pure SnO_2 are 6.053 g/cm^3 and $1.84 \times 10^{-6}\ \Omega^{-1}\ cm^{-1}$, respectively. The introduced Ti^{4+} can make the SnO_2 lattice more compact decreasing the lattice parameters [24], possibly due to the shorter Ti–O bond [25]. Hence, the doped SnO_2 has a higher density than the undoped SnO_2. In addition to the higher density, the Ti^{4+}-doped SnO_2 powders possess electrical conductivity that is 10^4 times higher than that of pure SnO_2. After Ti^{4+} incorporation into the SnO_2 lattice, the electric resistance decreases [26–28]. In fact, SnO_2 is an n-type semiconductor in which the intrinsic oxygen vacancies (Vő) are compensated by electrons. The equilibrium between oxygen vacancies and electrons is responsible for the semiconducting characteristics of SnO_2. The mechanism of can be expressed by the following equation [29]:

$$SnO_2 \rightarrow Sn''_{Sn} + Vő + O^x_O + \tfrac{1}{2}O_2. \quad (2)$$

As the ionic radius of Ti^{4+} (0.068 nm) is close to that of Sn^{4+} (0.071 nm), it is easy for Ti^{4+} to be doped into the crystal lattice of SnO_2 and occupy the substitutional positions [30]. This can create a large number of oxygen vacancies and increase the electrical conductivity of SnO_2. The process is shown in the equation:

$$Ti^{4+} \xrightarrow{SnO_2} Ti''_{Sn} + Vő. \quad (3)$$

In general, the electrical conductivity of the materials is determined by the following equation:

$$\sigma = c(ze)^2 b, \quad (4)$$

where σ is the electrical conductivity, c the concentration of charge carriers, z the chemical valence of charge carriers, e the charge of electron and b is the drift velocity of charge carriers. It is obvious that c increases significantly with Ti^{4+} doping according to Eq. (3). Therefore, the electrical conductivity (σ) of Ti^{4+} doped SnO_2 is improved significantly, which is in good agreement with our results.

4. Conclusion

We have demonstrated the fabrication of nano-sized Ti^{4+}-doped SnO_2 powders using the sol–gel technique. Polyethylene glycol (PEG) can effectively prevent the SnO_2 grains from agglomerating during the formation of the gel. We have obtained high quality Ti^{4+}-doped SnO_2 crystals and fine grains after Ti^{4+}-doped SnO_2 gel is sintered at 500 °C. After secondary calcination at 1000 °C, the Ti^{4+}-doped SnO_2 samples exhibit higher density and electrical conductivity. Our test results reveal that the doped materials possess significantly enhanced electrical conductivity and density compared to the undoped SnO_2 materials made by conventional methods.

Acknowledgement

The work was financially supported by City University of Hong Kong Directl Allocation Research Grant No. 9360110.

References

[1] B. Gengenbach, U. Mayer, R. Michal, K. Saeger, IEEE Trans. Comp. Hybrids Manuf. Technol. 8 (1985) 58–63.
[2] P.C. Wingert, C.H. Leung, IEEE Trans. Comp. Hybrids Manuf. Technol. 12 (1989) 16–20.
[3] M. Huck, A. Kraus, R. Michal, K.E. Saeger, Proceedings of the 15th ICEC, 1990, pp. 133–138.
[4] K.H. Schroder, IEEE Trans. Comp. Hybrids Manuf. Technol. 10 (1987) 127–134.
[5] C. Lambert, D. Weber, S. Coupez, J.P. Guerlet, Proceedings of the 35th IEEE Holm Conference Electr. Contacts, 1989, pp. 69–78.
[6] V. Behrens, T. Honig, A. Kraus, R. Michal, K.E. Saeger, R. Schmidberger, T. Staneff, Proceedings of the 39th IEEE Holm Conference Electr. Contacts, 1993, pp. 19–25.
[7] P. Wingert, C.H. Leung, IEEE Trans. Comp. Hybrids Manuf. Technol. 10 (1987) 56–62.
[8] D. Jeannot, J. Pinard, P. Ramoni, E.M. Jost, IEEE Trans. Comp. Hybrids Manuf. Technol. 17 (1994) 17–23.
[9] B. Gengenbach, R. Michal, G. Horn, IEEE Trans. Comp. Hybrids Manuf. Technol. 8 (1985) 64–69.
[10] H.Y. Liu, Y.P. Wang, B.J. Ding, Rare Met. Mater. Eng. 31 (2002) 122–124.
[11] M.Z. Rong, Q.P. Wang, Proceedings of the 39th IEEE Holm Conference Electr. Contacts, 1993, pp. 33–36.
[12] P.G. Slade, Y.K. Chien, J.A. Bindas, IEEE Trans. Comp. Hybrids Manuf. Technol. 13 (1990) 2–12.
[13] M.M. Oliveira, D.C. Schnitzler, A.J.G. Zarbin, Chem. Mater. 15 (2003) 1903–1909.
[14] J.C. Zhang, Q. Li, W.L. Cao, J. Mater. Sci. Technol. 21 (2005) 191–195.
[15] K. Zakrzewska, Thin Solid Films 391 (2001) 229–238.
[16] S. Taruta, K. Sakatsume, Y. Itou, N. Takusagawa, K. Okasa, N. Otsuka, in: R.S.T.C. Smart, J. Nowotny (Eds.), Ceramic Intersurfaces Properties and Applications, IOM Communications Ltd., London, 1998, pp. 367–386.
[17] ASTM B 328, Standard Test Method for Density and Interconnected Porosity of Sintered Metal Powder Structural Parts and Oil Impregnated Bearings g and Materials, American Society for Testing and Materials, 1983.
[18] International Standards Organization Standard ISO 2738. American National Standards Institute, New York, 1982.
[19] J. Yang, J.S. Lian, Q.Z. Dong, Q.F. Guan, J.W. Chen, Z.X. Guo, Mater. Lett. 57 (2003) 2792–2797.
[20] J.K. Ferri, Kathleen J. Stebe, Adv. Colloid Interface Sci. 85 (2000) 61–67.
[21] S.B. Qadri, E.F. Skelton, D. Hsu, A.D. Dinsmore, J. Yang, H.F. Gray, B.R. Ratna, Phys. Rev. B 60 (1999) 9191–9193.
[22] Z.W. Chen, J.K.L. Lai, C.H. Shek, J. Non-Cryst. Solids 351 (2005) 3619–3623.
[23] A. Cirera, A. Dieguez, R. Diaz, J.R. Morante, Sens. Actuators B 58 (1999) 360–364.
[24] M. Radecka, K. Zakrzewska, M. Rekas, Sens. Actuators B 47 (1998) 194–204.
[25] W. Lin, Y.F. Zhang, K.N. Ding, J.Q. Li, Y.J. Xu, J. Chem. Phys. 124 (2006), Art. No. 054704.
[26] S.F.A. Kettle, Physical Inorganic Chemistry, Oxford University Press, 2000.
[27] John A. Pople, Approximate Molecular Orbital Theory, McGraw-Hill, 1970.
[28] G.V. Samsonov, The Oxide Handbook, second ed., IFI/Plenum Data Company, New York, 1982.
[29] E.R. Leite, A.M. Nascimento, P.R. Bueno, E. Longo, J. Mater. Sci.-Mater. El 10 (1999) 321–327.
[30] G. Zhang, M.L. Liu, Sens. Actuators B 69 (2000) 144–152.